ELSEVIER

International Journal of Solids and Structures 40 (2003) 7513–7537

INTERNATIONAL JOURNAL OF SOLIDS and STRUCTURES

www.elsevier.com/locate/ijsolstr

Modeling quasi-static crack growth with the extended finite element method Part I: Computer implementation

N. Sukumar [a,*], J.-H. Prévost [b]

[a] *Department of Civil and Environmental Engineering, University of California, One Shields Avenue, Davis, CA 95616, USA*
[b] *Department of Civil and Environmental Engineering, Princeton University, Princeton, NJ 08544, USA*

Received 30 October 2002; received in revised form 30 May 2003

Abstract

The extended finite element method (X-FEM) is a numerical method for modeling strong (displacement) as well as weak (strain) discontinuities within a standard finite element framework. In the X-FEM, special functions are added to the finite element approximation using the framework of partition of unity. For crack modeling in isotropic linear elasticity, a discontinuous function and the two-dimensional asymptotic crack-tip displacement fields are used to account for the crack. This enables the domain to be modeled by finite elements without explicitly meshing the crack surfaces, and hence quasi-static crack propagation simulations can be carried out without remeshing. In this paper, we discuss some of the key issues in the X-FEM and describe its implementation within a general-purpose finite element code. The finite element program `Dynaflow`™ is considered in this study and the implementation for modeling 2-d cracks in isotropic and bimaterial media is described. In particular, the array-allocation for enriched degrees of freedom, use of geometric-based queries for carrying out nodal enrichment and mesh partitioning, and the assembly procedure for the discrete equations are presented. We place particular emphasis on the design of a computer code to enable the modeling of discontinuous phenomena within a finite element framework.

Keywords: Strong discontinuities; Partition of unity; Extended finite element; Finite element programming; Crack modeling; Singularity

1. Introduction

A problem of significant interest and importance in solid mechanics is the modeling of fracture and damage phenomena. These material failure processes manifest themselves in quasi-brittle materials such as rocks and concrete as fracture process zones, shear (localization) bands in ductile metals, or discrete crack discontinuities in brittle materials. The accurate modeling and the evolution of smeared and discrete

* Corresponding author. Tel.: +1-530-7546415; fax: +1-530-7527872.
E-mail address: nsukumar@ucdavis.edu (N. Sukumar).

0020-7683/$ - see front matter © 2003 Elsevier Ltd. All rights reserved.
doi:10.1016/j.ijsolstr.2003.08.002

discontinuities has been a topic of growing interest over the past few decades, with quite a few notable developments in computational techniques over the past few years.

Early numerical models for treating discontinuities in finite elements can be traced to the work of Ortiz et al. (1987) and Belytschko et al. (1988). They modeled shear bands as 'weak' (strain) discontinuities that could pass through finite elements using a multi-field variational principle. Dvorkin et al. (1990) considered 'strong' (displacement) discontinuities by modifying the principle of virtual work statement, whereas Lotfi and Sheng (1995) extended the three-field Hu–Washizu variational statement for bodies with internal discontinuities. A unified framework for analyzing strong discontinuities by taking into account the softening constitutive law and the interface traction–displacement relation was put forth by Simo and co-workers (Simo et al., 1993; Simo and Oliver, 1994). Applications and extensions of this approach have been proposed by many researchers for pre- as well as post-localization analyses (Armero and Garikipati, 1996; Sluys and Berends, 1998; Larsson and Runesson, 1996; Larsson et al., 1999; Regueiro and Borja, 2001; Bolzon and Corigliano, 2000). Borja (2000) presented a standard Galerkin formulation of the strong discontinuity approach and has shown its equivalence to assumed enhanced strain approximations.

In the strong discontinuity approach, the displacement consists of regular and enhanced components, where the enhanced component yields a jump across the discontinuity surface. An assumed enhanced strain variational formulation is used, and the enriched degrees of freedom are statically condensed on an element level to obtain the tangent stiffness matrix for the element. A comprehensive review and comparison of various embedded discontinuity approaches is provided by Jirásek (2000). An alternative approach to modeling fracture phenomena is the cohesive surface formulation of Xu and Needleman (1994), which has been used to model damage in brittle materials (Camacho and Ortiz, 1996). The cohesive surface formulation is a phenomenological framework in which the fracture characteristics of the material are embedded in a cohesive surface traction–displacement relation. Using this approach, an inherent length scale is introduced into the model, and in addition no fracture criterion (K-dominant field) is required; crack growth and the crack path are outcomes of the analysis.

A significant improvement in crack modeling was realized with the development of a partition-of-unity based enrichment method for discontinuous fields (Moës et al., 1999), which was referred to as the extended finite element method (X-FEM) (Dolbow, 1999; Daux et al., 2000). In the X-FEM, special functions are added to the finite element approximation using the framework of partition of unity (Melenk and Babuška, 1996; Duarte and Oden, 1996). For crack modeling, a discontinuous function (generalized Heaviside step function) and the two-dimensional linear elastic asymptotic crack-tip displacement fields are used to account for the crack. This enables the domain to be modeled by finite elements without explicitly meshing the crack surfaces. The location of the crack discontinuity can be arbitrary with respect to the underlying finite element mesh, and quasi-static or fatigue crack propagation simulations can be performed without the need to remesh as the crack advances. A particularly appealing feature is that the finite element framework and its properties (sparsity and symmetry) are retained, and a single-field (displacement) variational principle is used to obtain the discrete equations. This technique provides an accurate and robust numerical method to model strong (displacement) discontinuities in 2-d (Moës et al., 1999; Daux et al., 2000) and 3-d (Sukumar et al., 2000), as well as weak (strain) discontinuities (Sukumar et al., 2001).

In this paper, we describe the main issues in the implementation of the X-FEM, and present a robust and simple means to incorporate it into a general-purpose finite element program. The finite element program `Dynaflow`™ (Prévost, 1983) is considered in this study and the methodology for modeling 2-d cracks in isotropic and bimaterial media is presented. The initial development of the X-FEM at Northwestern University and the many recent advances of the method have all been carried out within a C++ code. However, since most existing finite element codes are in `Fortran`, we undertake the task to outline the X-FEM implementation within such a programming environment. The main contributions in this paper are:

- To provide a detailed account of the main issues that arise in the implementation of the X-FEM, and how to incorporate them within an existing finite element code so that apart from crack modeling, the incorporation of other types of discontinuities will also become apparent.
- Design of data structures for variable *nodal degrees of freedom* array and for the assembly of the discrete equations. The computational algorithms to select the enriched nodes and to compute the enrichment functions are described. The need for *partitioning of elements* is addressed, and its distinction from *remeshing* is pointed out.
- Step-by-step treatment of the assembly procedure of the bilinear form for elements that are cut by the crack; this aspect has not been described in earlier works. In addition, details on the submatrices and vectors that arise in the global stiffness matrix and external force vector are provided.

In Section 2, the extended finite element method is introduced and recent applications of the method in mechanics and materials science are mentioned. Crack modeling in the X-FEM is discussed in Section 2.1. The implementation of the X-FEM within `Dynaflow`™ is outlined in Section 3, and a few concluding remarks are made in Section 4.

2. Extended finite element method

The partition of unity method (Melenk and Babuška, 1996; Duarte and Oden, 1996) generalized finite element approximations by presenting a means to embed local solutions of boundary-value problems into the finite element approximation. This idea was first exploited by Oden and co-workers (Oden et al., 1998; Duarte et al., 1998) for problems with internal boundaries—the numerical technique was termed as the generalized finite element method (GFEM). Strouboulis et al. (2000) used local enrichment functions in the GFEM for modeling re-entrant corners and holes, whereas Duarte et al. (2001) simulated dynamic crack propagation in 3-d using the partition of unity framework. A comprehensive summary of the GFEM appears in Strouboulis et al. (2001).

In Belytschko and Black (1999), the partition of unity enrichment for crack discontinuities and near-tip crack fields was introduced. The enrichment functions for crack problems are functions that span the asymptotic near-tip displacement field—see Fleming et al. (1997) for their use in the element-free Galerkin method (Belytschko et al., 1994). A notable improvement and progress in discrete crack growth modeling without the need for any remeshing strategy was conceived in Moës et al. (1999). The generalized Heaviside function was proposed as a means to model the crack away from the crack-tip, with simple rules for the introduction of the discontinuous and crack-tip enrichments. This advance has provided a robust and accurate computational tool for modeling discontinuities independent of the crack geometry. The partition of unity framework satisfies a few key properties which renders it as a powerful tool for local enrichment within a finite element setting:

1. can include application-specific basis functions to better approximate the solution;
2. automatic enforcement of continuity (conforming trial and test approximations); and
3. point or line singularities as well as surface discontinuities can be handled without the need for the discontinuous surfaces to be aligned with the finite element mesh.

The above properties are in sharp contrast to enriched finite elements (Benzley, 1974; Gifford and Hilton, 1978; Ayhan and Nied, 2002), where transition elements are required to satisfy displacement continuity. In classical as well as enriched finite element methods, remeshing is required to conduct crack growth simulations.

The X-FEM has been successfully applied to 2-dimensional static and quasi-static crack growth problems (Moës et al., 1999; Dolbow, 1999; Dolbow et al., 2000a,b; Dolbow et al., 2001; Moës and Belytschko, 2002), with its extension to modeling holes, and branched and intersecting cracks proposed in Daux et al. (2000). The application of this technique for 3-dimensional crack problems was presented in Sukumar et al. (2000). The interface of the X-FEM with level set techniques to model weak discontinuities such as material interfaces (bimaterials) was introduced in Sukumar et al. (2001), whereas the representation of tangential discontinuities was presented in Belytschko et al. (2001). Recent studies have explored the use of fast marching and level sets for evolving crack discontinuities in 2-dimensions (Stolarska et al., 2001) and 3-dimensions within the X-FEM framework. The growth of multiple coplanar cracks in 3-d is handled using the fast marching method (Sukumar et al., 2003a; Chopp and Sukumar, 2003), whereas non-planar crack growth is carried out using level sets (Moës et al., 2002; Gravouil et al., 2002).

The X-FEM has also been utilized to model computational phenomena in areas such as fluid mechanics, phase transformations, and materials science. In Wagner et al. (2001), a computational model for rigid particles in Stokes flow was proposed, whereas moving phase boundary problems have been modeled using the coupled extended finite element and level set methods (Merle and Dolbow, 2002; Ji et al., 2002; Chessa et al., 2002). Dolbow and Nadeau (2002) investigated the use of effective properties for fracture analysis in functionally-graded systems, whereas Sukumar et al. (2003b) adopted the X-FEM as a fracture tool to study the competition between intergranular and transgranular modes of crack growth through a material microstructure. In other related studies, Wells and Sluys (2001) used the Heaviside step function to model the displacement discontinuity within a finite-element based cohesive crack model, whereas Wells et al. (2002) used partition of unity enrichment to alleviate volumetric locking during plastic flow.

2.1. Crack modeling in two-dimensions

In finite elements, a basis function N_I is associated with node I in the mesh. Let $\omega_I = \{\mathbf{x} : N_I(\mathbf{x}) > 0\}$ be the region of support for N_I. The nodes belonging to an element are given by the connectivity of the element, whereas its dual ω_I, is the collection of elements that are associated with a specific node I (see Fig. 1).

In the X-FEM, a crack is represented by enriching the classical displacement-based finite element approximation through the framework of partition of unity (Melenk and Babuška, 1996). A crack is modeled by enriching the nodes whose nodal shape function support intersects the interior of the crack by a discontinuous function, and enriching the nodes whose nodal shape function supports intersect the crack-tip by the two-dimensional linear elastic asymptotic near-tip fields. Additional degrees of freedom are associated with nodes that are enriched. Partitioning algorithms are also implemented if the crack intersects the finite elements. We first present the enrichment functions used for crack modeling and the criteria for the selection of the enriched nodes. Then, the need for element partitioning is discussed and lastly, the discrete equations are presented.

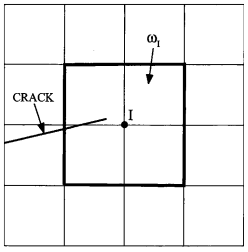

Fig. 1. Support ω_I (dark line) for a nodal shape function.

2.1.1. Enrichment functions

We will use lower case and upper case bold-faced letters to denote vectors and matrices, respectively. The Cartesian coordinate axes are denoted by $\mathbf{x} \equiv (x, y)$ in 2-d, with Latin lower case indices referring to Cartesian components. Nodes in the finite element mesh are denoted by Latin subscripts—lower case indices refer to the local node number within an element whereas upper case indices are used for the global node number in the mesh (Hughes, 1987). Consider a body $\Omega \subset \mathbb{R}^2$ that contains an internal traction-free crack (Fig. 2). For a single crack in 2-dimensions, let Γ_c be the crack surface (interior) and Λ_c the crack tip(s)—the closure $\overline{\Gamma}_c = \Gamma_c \cup \Lambda_c$. The description of the enrichment functions follows:

Generalized Heaviside function. The interior of a crack (Γ_c is the enrichment-domain) is modeled by the generalized Heaviside enrichment function H, where H takes on the value +1 above the crack and −1 below the crack (Moës et al., 1999):

$$H(\mathbf{x}) = \begin{cases} 1 & \text{if } (\mathbf{x} - \mathbf{x}^*) \cdot \mathbf{n} \geqslant 0, \\ -1 & \text{otherwise,} \end{cases} \tag{1}$$

where $\mathbf{x}$ is a sample (Gauss) point, $\mathbf{x}^*$ (lies on the crack) is the closest point to $\mathbf{x}$, and $\mathbf{n}$ is the unit outward normal to the crack at $\mathbf{x}^*$.

Near-tip crack functions. To model the crack-tip and also to improve the representation of crack-tip fields in fracture computations, crack-tip enrichment functions are used in the element which contains the crack tip. The crack-tip enrichment consists of functions which incorporate the radial and angular behavior of the two-dimensional asymptotic crack-tip displacement field. The use of the crack-tip functions serves two main purposes:

1. If the crack were to terminate in the interior of an element, then enriching the crack-tip element with the Heaviside function would be inaccurate. This is so, since by such a choice the crack would be modeled as though the segment containing the crack-tip were extended till it intersected the element edge. The crack-tip enrichment functions ensure that the crack terminates precisely at the location of the crack-tip, and hence these functions are required to model the crack for this case.
2. The use of the linear elastic (or bimaterial) asymptotic crack-tip fields serve as suitable enrichment functions for they possess the correct near-tip behavior, and in addition, their use also leads to better accuracy on relatively coarse finite element meshes in 2-d (Moës et al., 1999; Daux et al., 2000; Huang et al., 2003a,b; Sukumar et al., 2003a) and 3-d (Sukumar et al., 2000).

The crack-tip enrichment functions in isotropic elasticity are (Fleming et al., 1997):

$$[\Phi_\alpha(\mathbf{x}), \alpha = 1\text{–}4] = \left[\sqrt{r}\sin\frac{\theta}{2}, \sqrt{r}\cos\frac{\theta}{2}, \sqrt{r}\sin\theta\sin\frac{\theta}{2}, \sqrt{r}\sin\theta\cos\frac{\theta}{2}\right], \tag{2}$$

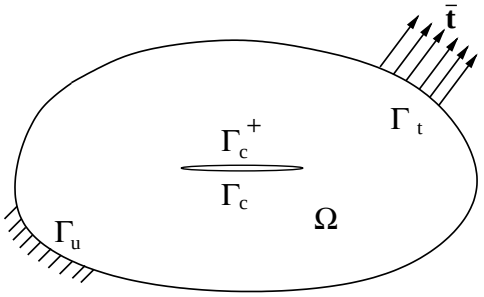

Fig. 2. Boundary value problem with an internal traction-free crack.

where r and θ are polar coordinates in the local crack-tip coordinate system. Note that the first function in the above equation is discontinuous across the crack. In Fig. 3, the shape function support ω_I as well as the local coordinate system for the crack-tip enrichment functions are illustrated.

The use of crack-tip functions is not restricted to crack modeling in isotropic media alone. Consider a bimaterial with a crack perpendicular to the interface (Fig. 4); the crack terminates at the interface. The near-tip asymptotic field for this problem has been studied by many researchers (Zak and Williams, 1963; Bogy, 1971; Cook and Erdogan, 1972; Chen, 1994). The elastic mismatch between the two elastic materials is characterized by Dundurs parameters (Dundurs, 1969):

$$\alpha = \frac{\mu_1(\kappa_2+1)-\mu_2(\kappa_1+1)}{\mu_1(\kappa_2+1)+\mu_2(\kappa_1+1)}, \quad \beta = \frac{\mu_1(\kappa_2-1)-\mu_2(\kappa_1-1)}{\mu_1(\kappa_2+1)+\mu_2(\kappa_1+1)}, \tag{3a}$$

$$\kappa_i = \begin{cases} \dfrac{3-\nu_i}{1+\nu_i} & \text{(plane stress)}, \\ 3-4\nu_i & \text{(plane strain)}, \end{cases} \tag{3b}$$

where μ_i and ν_i are the shear modulus and the Poisson's ratio, respectively, of material i ($i = 1, 2$).

The asymptotic displacement field near the tip of a plane strain crack in a bimaterial takes the form (Chen, 1994)

$$\mathbf{u}_i(r,\theta) = r^{1-\lambda}\{\mathbf{a}_i \sin\lambda\theta + \mathbf{b}_i \cos\lambda\theta + \mathbf{c}_i \sin(\lambda-2)\theta + \mathbf{d}_i \cos(\lambda-2)\theta\}, \tag{4}$$

where λ ($0 < \lambda < 1$), which is the stress singularity exponent, is a function of the Dundurs parameters and is given by the root of the transcendental equation (Zak and Williams, 1963)

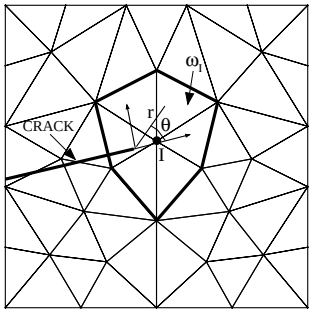

Fig. 3. Coordinate configuration (r, θ) for crack tip enrichment functions.

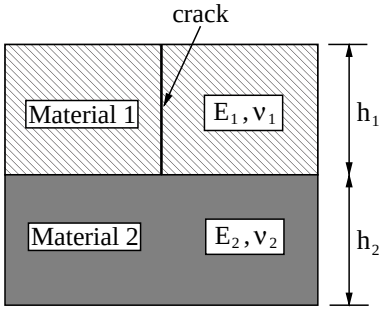

Fig. 4. Bimaterial with a crack impinging on the interface.

$$\cos(\lambda\pi) - 2\frac{\alpha-\beta}{1-\beta}(1-\lambda)^2 + \frac{\alpha-\beta^2}{1-\beta^2} = 0. \tag{5}$$

The value of λ as a function of α and β is tabulated in Beuth (1992). In the case of no mismatch ($\alpha = \beta = 0$), the stress singularity reduces to the classical inverse $\sqrt{r}$ stress singularity ($\lambda = 1/2$) for homogeneous linear elastic materials. When material 2 is stiffer than material 1 ($\alpha < 0$), the singularity is weaker ($\lambda < 1/2$), and if material 2 is more compliant than material 1 ($\alpha > 0$), the singularity is stronger ($\lambda > 1/2$).

The crack-tip enrichment functions for the bimaterial crack problem are (Huang et al., 2003a,b):

$$[\Psi_\alpha(\mathbf{x}), \alpha = 1\text{–}4] = \left[r^{1-\lambda}\sin\lambda\theta, r^{1-\lambda}\cos\lambda\theta, r^{1-\lambda}\sin(\lambda-2)\theta, r^{1-\lambda}\cos(\lambda-2)\theta\right], \tag{6}$$

where the above functions span the asymptotic crack-tip displacement expansion given in Eq. (4). Note that in this instance the first function and the third function in the above equation are discontinuous across the crack ($\theta = \pm\pi$). Recently, partition of unity enrichment for modeling bimaterial interface cracks has also been developed within Dynaflow™; see Sukumar et al. (in press) for details.

2.1.2. Selection of enriched nodes

The approximation for a vector-valued function $\mathbf{u}$ with the partition of unity enrichment is of the general form (Melenk and Babuška, 1996):

$$\mathbf{u}^h(\mathbf{x}) = \sum_{I=1}^{N} N_I(\mathbf{x})\left(\sum_{\alpha=1}^{M}\psi_\alpha(\mathbf{x})\mathbf{a}_I^\alpha\right), \tag{7}$$

where N_I are the finite element shape functions and ψ_α are the enrichment functions. The finite element shape functions form a partition of unity: $\sum_I N_I(\mathbf{x}) = 1$. From Eq. (7), we note that the finite element space ($\psi_1 \equiv 1$; $\psi_\alpha = 0$ $(\alpha \neq 1)$) is a subspace of the enriched space.

In the particular instance of 2-d crack modeling, the enriched displacement (trial and test) approximation is written as (Moës et al., 1999):

$$\mathbf{u}^h(\mathbf{x}) = \sum_{I\in\mathcal{N}} N_I(\mathbf{x})\left[\mathbf{u}_I + \underbrace{H(\mathbf{x})\mathbf{a}_I}_{I\in\mathcal{N}_\Gamma} + \underbrace{\sum_{\alpha=1}^{4}\Phi_\alpha(\mathbf{x})\mathbf{b}_I^\alpha}_{I\in\mathcal{N}_\Lambda}\right], \tag{8}$$

where $\mathbf{u}_I$ is the nodal displacement vector associated with the continuous part of the finite element solution, $\mathbf{a}_I$ is the nodal enriched degree of freedom vector associated with the Heaviside (discontinuous) function, and $\mathbf{b}_I^\alpha$ is the nodal enriched degree of freedom vector associated with the elastic asymptotic crack-tip functions. In the above equation, $\mathcal{N}$ is the set of all nodes in the mesh; $\mathcal{N}_\Gamma$ is the set of nodes whose shape function support is cut by the crack interior Γ_c; and $\mathcal{N}_\Lambda$ is the set of nodes whose shape function support is cut by the crack tip Λ_c ($\mathcal{N}_\Gamma \cap \mathcal{N}_\Lambda = \emptyset$):

$$\mathcal{N}_\Lambda = \{n_K : n_K \in \mathcal{N}, \bar{\omega}_K \cap \Lambda_c \neq \emptyset\}, \tag{9a}$$

$$\mathcal{N}_\Gamma = \{n_J : n_J \in \mathcal{N}, \omega_J \cap \Gamma_c \neq \emptyset, n_J \notin \mathcal{N}_\Lambda\}. \tag{9b}$$

For any node in $\mathcal{N}_\Gamma$, the support of the nodal shape function is fully cut into two disjoint pieces by the crack. If for a certain node n_I, one of the two pieces is very small compared to the other, then the generalized Heaviside function used for the enrichment is almost a constant over the support, leading to an ill-conditioned stiffness matrix (Moës et al., 1999). Therefore, in this case, node n_I is removed from the set $\mathcal{N}_\Lambda$. The *area-criterion* for nodal inclusion in $\mathcal{N}_\Lambda$ is as follows: The area above the crack is A_ω^{above}, and the area below the crack is A_ω^{below} : $A_\omega = A_\omega^{\text{above}} + A_\omega^{\text{below}}$. If either of the two ratios, $A_\omega^{\text{above}}/A_\omega$ or $A_\omega^{\text{below}}/A_\omega$ is below a

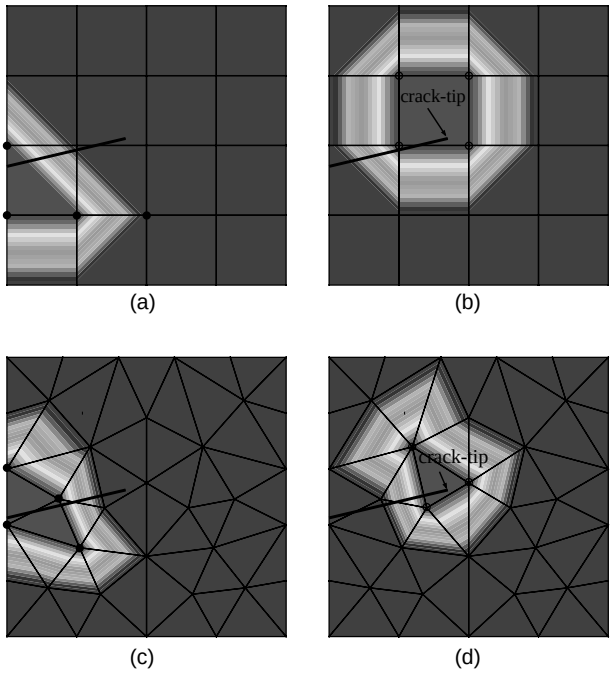

Fig. 5. Heaviside and near-tip nodal enrichment for a 2-d edge-crack problem. The Heaviside enriched nodes are shown in filled circles, the near-tip enriched nodes are shown in open circles, and the enrichment region can be inferred from the contour plot, where the contour value on an enriched node is unity and zero on all other nodes. (a) Heaviside enrichment for regular (rectangular) mesh; (b) Near-tip enrichment for regular (rectangular) mesh; (c) Heaviside enrichment for unstructured (triangular) mesh; and (d) Near-tip enrichment for unstructured (triangular) mesh.

prescribed tolerance, the node is removed from the set $\mathscr{N}_A$ (Dolbow et al., 2000a). A tolerance $\epsilon = 10^{-4}$ is used in the computations.

The enriched nodes for the interior of a crack and those for the crack tip are shown in Fig. 5. From the contours shown in Fig. 5, one can also infer the region (union of elements) over which the enriched basis functions are non-zero.

2.1.3. Element partitioning versus remeshing

If a crack intersects an element, the element is subdivided into triangles (in 2-d) such that element edges are coincident with the crack geometry. We elaborate on this point, since a common misconception has been that such a procedure is unnecessary, and if it were indeed a requirement, then in essence *remeshing* is being carried out. We clarify both these issues.

Referring to Fig. 2, we multiply the strong form of the boundary-value problem by test functions $\delta\mathbf{u} \in H_0^1(\Omega)$ to obtain:

$$\int_\Omega (\nabla \cdot \boldsymbol{\sigma}) \cdot \delta\mathbf{u}\, \mathrm{d}\Omega + \int_\Omega \mathbf{b} \cdot \delta\mathbf{u}\, \mathrm{d}\Omega = 0, \tag{10}$$

where $\mathbf{b}$ is the body force per unit volume, $\boldsymbol{\sigma}$ is the Cauchy stress, δ is the first variation operator, $H_0^1(\Omega)$ is the Sobolev space of functions with square-integrable derivatives that vanish on the essential boundary, and Ω is the open set that does not contain the crack surfaces. The above equation is re-written as

$$\int_{\Omega} \nabla \cdot (\boldsymbol{\sigma} \cdot \delta\mathbf{u})\, \mathrm{d}\Omega - \int_{\Omega} \boldsymbol{\sigma} : \nabla(\delta\mathbf{u})\, \mathrm{d}\Omega + \int_{\Omega} \mathbf{b} \cdot \delta\mathbf{u}\, \mathrm{d}\Omega = 0, \tag{11}$$

and on using the divergence (Green's) theorem in Ω and the symmetry of $\boldsymbol{\sigma}$, we have

$$\int_{\Gamma_t \cup \Gamma_u} \mathbf{t} \cdot \delta\mathbf{u}\, \mathrm{d}\Gamma + \int_{\Gamma_c^+ \cup \Gamma_c^-} \mathbf{t} \cdot \delta\mathbf{u}\, \mathrm{d}\Gamma - \int_{\Omega} \boldsymbol{\sigma} : \delta\boldsymbol{\varepsilon}\, \mathrm{d}\Omega + \int_{\Omega} \mathbf{b} \cdot \delta\mathbf{u}\, \mathrm{d}\Omega = 0, \tag{12}$$

where $\boldsymbol{\varepsilon} = \mathbf{u}_{(\ )}$ denotes the symmetric part of the displacement gradient (small strain tensor). Since $\mathbf{t} = \boldsymbol{\sigma} \cdot \mathbf{n} = \bar{\mathbf{t}}$ (prescribed traction) on Γ_t, $\mathbf{t} \equiv 0$ on $\Gamma_c^{\pm}$ (traction-free crack faces), and by choosing test functions that vanish on the essential boundary Γ_u, we obtain the weak form (principle of virtual work) for the continuous problem as:

$$\int_{\Omega} \boldsymbol{\sigma} : \delta\boldsymbol{\varepsilon}\, \mathrm{d}\Omega = \int_{\Gamma_t} \bar{\mathbf{t}} \cdot \delta\mathbf{u}\, \mathrm{d}\Gamma + \int_{\Omega} \mathbf{b} \cdot \delta\mathbf{u}\, \mathrm{d}\Omega \quad \forall \delta\mathbf{u} \in H_0^1(\Omega). \tag{13}$$

In the above derivation, the divergence theorem is used which is applicable to a domain in which u_i is sufficiently regular (must not contain discontinuities or singularities), and hence the crack surfaces must be an internal boundary of the domain of integration. In the weak statement for the finite element (discrete) problem, the domain Ω must be divided into non-overlapping subdomains (elements Ω_e) that must conform to the same requirement as that in the continuous problem. This provides equivalence between the strong and weak statements of the boundary-value problem.

We can now infer that the discrete weak form demands that element edges must conform to the crack geometry. If this requirement is not met, then the equivalence between the strong form and the weak form is lost. If we choose to ignore this fact and do not partition an element that is cut by a crack (see Fig. 6), then numerical difficulties also arise. For crack modeling, the classical finite element space is enriched by a discontinuous (Heaviside) function H and the near-tip asymptotic fields. The X-FEM approximation is provided in Eq. (8), and the enrichment functions for isotropic media are given in Eqs. (1) and (2). From Eq. (13), we note that the integrand in the discrete approximation for the bilinear form would consist of product of basis function derivatives. The derivatives of the enriched basis functions are discontinuous across the crack. [1] Hence, if the element shown in Fig. 6 is not subdivided, the numerical integration of a discontinuous function is involved. A well-known recipe in multi-dimensional integration over simplexes is to place line singularities and discontinuities along edges and point singularities at vertices of simplexes. If discontinuities are present within a simplex, then the use of Gauss quadrature rules will prove to be inaccurate for such integrals. To illustrate this, we consider a discontinuous function and a piece-wise continuous function that are defined in $\Omega = (-1/2, 1)$ (Fig. 7). We define the integral $I[f]$ as:

$$I[f] := \int_{\Omega} f(x)\, \mathrm{d}x \tag{14}$$

and consider the Gauss quadrature formula $Q[f]$:

$$I[f] \simeq Q[f] := \mathscr{J} \sum_{k=1}^{nsp} w_k f(\xi_k), \tag{15}$$

where $x = x(\xi)$ is the linear map with $\xi \in (-1, 1)$ the reference coordinate. In addition, the Jacobian $\mathscr{J} = \mathrm{d}x/\mathrm{d}\xi = 3/4$, and w_k and ξ_k are the Gauss points and weights for a *nsp*-order Gauss integration rule.

[1] Referring to Fig. 6, we point out that $(N_I H)_{,i}$ would also consist of a term $N_I \delta_{\Gamma_c} \mathbf{n} \cdot \mathbf{e}_i$ ($\mathbf{n}$ is the unit normal to the crack and δ_{Γ_c} is the δ-distribution); we do not consider this term since products of such terms that would appear in the bilinear form are non-integrable in the Lebesgue sense.

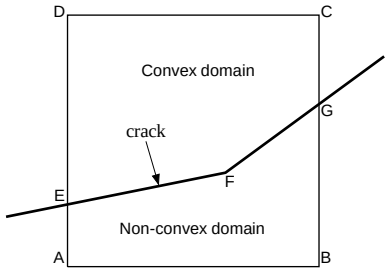

Fig. 6. Intersection of a crack with a finite element.

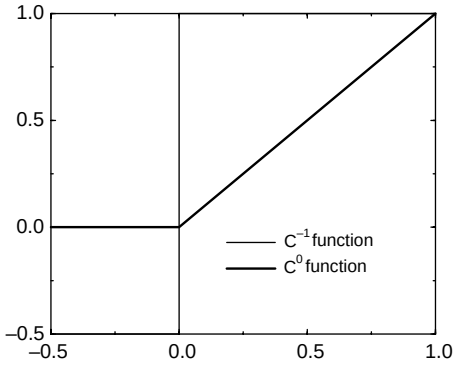

Fig. 7. C^{-1} (discontinuous) and C^0 (ramp) functions.

The exact value of the integrals are: $I[f] = 3/4$ and $I[f] = 1/2$ for the jump function and the piece-wise linear function, respectively. In Table 1, the results obtained using Gauss quadrature are presented for different values of *nsp*. It is evident that Gauss quadrature rules prove to be inadequate for the integration of such functions. However, if the domain is subdivided: $\Omega = \Omega_1 \cup \Omega_2 \equiv (-1/2, 0) \cup (0, 1)$, and then Eq. (15) is applied to each subdomain, the exact solution is recovered. On the basis of the above discussion, we infer that the crack geometry must coincide with edges of simplexes used in the numerical integration. From Fig. 6, we note that this can be achieved by carrying out numerical integration on the convex subdomain

Table 1
Numerical integration of discontinuous and piece-wise continuous functions

$f(x)$	No. of Gauss points (*nsp*)	$Q[f]$	$I[f]$
C^{-1}	1	1.5000	0.75
	2	0.3750	
	5	0.6950	
	7	0.6101	
	10	0.7075	
C^0	1	0.3750	0.5
	2	0.5123	
	5	0.5066	
	7	0.4996	
	10	0.5015	

CDEFG and the non-convex subdomain *ABGFE*. The design and development of quadrature rules over arbitrary polygons has not yet reached a mature stage; for the difficulties associated with this endeavor and recent progress achieved in this direction, see Rashid and Gullett (2000). The partitioning of the convex and non-convex subdomains into triangles is a simple task which then permits the use of well-known quadrature rules for triangles. In essence, this is an elegant and tractable means to judiciously choose the location of integration points and their weights to perform numerical integration on arbitrary polygons. Hence, the theoretical issues notwithstanding, from a purely computational viewpoint, the partitioning of elements that are cut by the crack is a viable and cost-effective approach to perform sufficiently accurate numerical integration.

We now delineate the distinction of the above partitioning procedure from a remeshing algorithm. Remeshing engenders the construction of a richer discrete space (better approximating power) by increasing the number of basis functions in the approximation. This is achieved by refining the mesh near a singularity (gradients are large in the vicinity of the singularity). The remeshing algorithm, however, must ensure that the derivatives of the basis functions in any element do not become very large. This is met by imposing certain restrictions on the shape of elements so that the *uniformity condition* on the basis functions is satisfied; badly shaped elements (e.g., triangular elements with obtuse angle close to π) impact accuracy and the rate of convergence of the finite element method. The partitioning procedure used in the X-FEM differs from remeshing in a few key aspects:

1. In the X-FEM, element partitioning is done solely for the purpose of numerical integration; no additional degrees of freedom are introduced into the discrete space.
2. No inherent restrictions are placed on the shape of the partitioned elements, since the basis functions (classical finite element as well as enriched) are associated with nodes that are tied to the parent element and not to the subtriangle. In Appendix A, we list a subroutine that is used to compute $(\xi,\eta)_{\square}$ ($\square$ is the bi-unit square).
3. The task of subdividing an element that is cut by a crack into triangles in 2-d or tetrahedra in 3-d is a relatively straight-forward exercise in computational geometry.

2.1.4. Discrete equations

From Eq. (13), the discrete weak form for linear elastostatics is:

$$\int_{\Omega^h} \boldsymbol{\sigma} : \delta\boldsymbol{\varepsilon}^h \,\mathrm{d}\Omega = \int_{\Omega^h} \mathbf{b}\cdot\delta\mathbf{u}^h \,\mathrm{d}\Omega + \int_{\partial\Omega_t^h} \bar{\mathbf{t}}\cdot\delta\mathbf{u}^h \,\mathrm{d}\Gamma \quad \forall\delta\mathbf{u}^h \in \mathbf{U}_0^h, \tag{16}$$

where $\mathbf{u}^h \in \mathbf{U}^h$ and $\delta\mathbf{u}^h \in \mathbf{U}_0^h$ are the approximating trial and test functions used in the X-FEM, and the linear elastic constitutive relation is: $\boldsymbol{\sigma} = \mathbf{D} : \boldsymbol{\varepsilon}$, where $\mathbf{D}$ is the constitutive matrix (plane stress or plane strain) for an isotropic linear elastic material. The finite element domain $\Omega^h = \cup_{e=1}^{m} \Omega_e^h$, where Ω_e^h is an element (or a subdivision of an element) such that the crack lies along the edges of these elements. On using the weak form as the starting point, Belytschko and Black (1999) showed that the discontinuous discrete approximation satisfies (in a weak sense) the traction-free conditions on the crack faces.

On substituting the X-FEM trial and test functions in the above equation, and using the arbitrariness of nodal variations, the following discrete system of linear equations is obtained:

$$\mathbf{K}\mathbf{d} = \mathbf{f}, \tag{17}$$

where $\mathbf{d}$ is the vector of nodal unknowns, and $\mathbf{K}$ and $\mathbf{f}$ are the global stiffness matrix and external force vector, respectively. The stiffness matrix and the force vector are computed on an element-by-element basis and assembled into their global counterparts through the usual assembly procedure (see Section 3.4 for details). The element contribution to $\mathbf{K}$ and $\mathbf{f}$ are as follows:

$$\mathbf{k}_{ij}^{e} = \begin{bmatrix} \mathbf{k}_{ij}^{uu} & \mathbf{k}_{ij}^{ua} & \mathbf{k}_{ij}^{ub} \\ \mathbf{k}_{ij}^{au} & \mathbf{k}_{ij}^{aa} & \mathbf{k}_{ij}^{ab} \\ \mathbf{k}_{ij}^{bu} & \mathbf{k}_{ij}^{ba} & \mathbf{k}_{ij}^{bb} \end{bmatrix}, \tag{18a}$$

$$\mathbf{f}_{i}^{e} = \{ \mathbf{f}_{i}^{u} \quad \mathbf{f}_{i}^{a} \quad \mathbf{f}_{i}^{b1} \quad \mathbf{f}_{i}^{b2} \quad \mathbf{f}_{i}^{b3} \quad \mathbf{f}_{i}^{b4} \}^{\mathrm{T}}, \tag{18b}$$

where the submatrices and vectors that appear in Eq. (18) are defined as:

$$\mathbf{k}_{ij}^{rs} = \int_{\Omega^e} (\mathbf{B}_i^r)^{\mathrm{T}} \mathbf{D} \mathbf{B}_j^s \, \mathrm{d}\Omega \quad (r,s = u,a,b) \tag{19a}$$

$$\mathbf{f}_{i}^{u} = \int_{\partial\Omega_t^h \cap \partial\Omega^e} N_i \bar{\mathbf{t}} \, \mathrm{d}\Gamma + \int_{\Omega^e} N_i \mathbf{b} \, \mathrm{d}\Omega, \tag{19b}$$

$$\mathbf{f}_{i}^{a} = \int_{\partial\Omega_t^h \cap \partial\Omega^e} N_i H \bar{\mathbf{t}} \, \mathrm{d}\Gamma + \int_{\Omega^e} N_i H \mathbf{b} \, \mathrm{d}\Omega, \tag{19c}$$

$$\mathbf{f}_{i}^{b\alpha} = \int_{\partial\Omega_t^h \cap \partial\Omega^e} N_i \Phi_\alpha \bar{\mathbf{t}} \, \mathrm{d}\Gamma + \int_{\Omega^h} N_i \Phi_\alpha \mathbf{b} \, \mathrm{d}\Omega \quad (\alpha = 1\text{–}4). \tag{19d}$$

In the above equations, N_i is the standard finite element shape function that is defined at node i ($i = 1, nen$) of the finite element, where *nen* is the number of nodes in the connectivity of the finite element. The number of degrees of freedom $ndof = 2$ in 2-d elasticity. Nodes in the set $\mathscr{N}_\Gamma$ have one enriched degree of freedom in each spatial dimension, and nodes in the set $\mathscr{N}_\Lambda$ have four enriched degrees of freedom in each spatial dimension—refer to Section 2.1.1. for details on the nodal sets $\mathscr{N}_\Gamma$ and $\mathscr{N}_\Lambda$.

In Eq. (19), $\mathbf{B}_i^u$, $\mathbf{B}_i^a$, and $\mathbf{B}_i^b$ are the matrix of shape function derivatives which are given by

$$\mathbf{B}_i^u = \begin{bmatrix} N_{i,x} & 0 \\ 0 & N_{i,y} \\ N_{i,y} & N_{i,x} \end{bmatrix}, \tag{20a}$$

$$\mathbf{B}_i^a = \begin{bmatrix} (N_i H)_{,x} & 0 \\ 0 & (N_i H)_{,y} \\ (N_i H)_{,y} & (N_i H)_{,x} \end{bmatrix}, \tag{20b}$$

$$\mathbf{B}_i^b = [\, \mathbf{B}_i^{b1} \quad \mathbf{B}_i^{b2} \quad \mathbf{B}_i^{b3} \quad \mathbf{B}_i^{b4} \,], \tag{20c}$$

$$\mathbf{B}_i^{b\alpha} = \begin{bmatrix} (N_i \Phi_\alpha)_{,x} & 0 \\ 0 & (N_i \Phi_\alpha)_{,y} \\ (N_i \Phi_\alpha)_{,y} & (N_i \Phi_\alpha)_{,x} \end{bmatrix} \quad (\alpha = 1\text{–}4). \tag{20d}$$

3. Computer implementation

The task of incorporating the X-FEM capabilities within a general-purpose finite element program can be broken down into the following subcategories:

1. Input data (crack geometry, enrichment types, crack growth law)
2. Nodal degrees of freedom

3. Mesh–geometry interactions (nodal enrichment and element partitioning)
4. Assembly procedure
5. Post-processing

The central ideas and issues that are described below are based on the original development of the X-FEM in Moës et al. (1999) and Daux et al. (2000), where C++ was used as the programming language and the tools developed within that framework were ideally-suited for the incorporation of many different applications within one code (Dolbow, 1999; Sukumar et al., 2001; Wagner et al., 2001; Sukumar et al., 2003a; Ji et al., 2002). In the present instance, we address similar issues and describe a means to incorporate the same capabilities within a `Fortran` programming environment—`Dynaflow`™ (Prévost, 1983) is considered in this study.

3.1. Input data

In finite elements, the finite element mesh is used to fully describe the model domain as well as the internal boundaries (defects such as holes and cracks). In the X-FEM, the problem domain is represented by a finite element mesh, whereas the internal boundaries such as cracks are not. The enriched displacement approximation given in Eq. (8) is used to account for the presence of the cracks in the model. In 2-dimensions, we represent cracks as piecewise linear segments, with the crack tip being a point in 2-space: each crack is defined by contiguous piecewise linear segments, i.e., $\Gamma_c = \cup_{i=1}^{p} \mathbf{l}_i$, where $\mathbf{l}_i = \{\mathbf{x}_a^i, \mathbf{x}_b^i\}$, with $\mathbf{x}_a^i = \mathbf{x}_b^{i-1}$ for $i = 2, 3, \ldots, p$. The crack-tip(s) are either or both of $\mathbf{x}_a^1$ and $\mathbf{x}_b^p$.

In the input data file, the crack geometry, enrichment type for the crack, and parameters for crack growth (evolution) are indicated. Keywords that have to appear verbatim in the data file are cast in `typewriter font`. A backslash (\) denotes continuation within a block, the text after an exclamation (!) is treated as comments, and a blank line denotes the end of a block. Each model is subdivided into regions (DEFINE_REGION) where the physical phenomenon in the region is typically described by a set of partial differential equations. In the finite element model, a region consists of a union of finite elements and the physics acting in the region is embedded within several ELEMENT_GROUP. This demarcation allows the integration of multi-physics processes (thermoelastic, fluid-structure, or poroelastic) to be readily simulated. Each region may consist of a link to several element groups—a crack is an element group with geometric properties (connectivity) and a material model (properties, parameters for stress intensity factor computation, crack growth law, etc.). A single crack is defined within one DEFINE_ELEMENT_GROUP block; multiple blocks are required for multiple crack definitions. Six different keywords have been defined for crack enrichment, namely

$$\texttt{enrichment\_type} = \begin{cases} \texttt{crack\_without\_tip} & \text{(Heaviside)}, \\ \texttt{crack\_with\_tip\_1} & \text{(Heaviside + crack functions at tip 1)}, \\ \texttt{crack\_with\_tip\_2} & \text{(Heaviside + crack functions at tip 2)}, \\ \texttt{crack} & \text{(Heaviside + crack fns at both tips)}, \\ \texttt{crack\_bimat\_tip\_1} & \text{(Heaviside + bimat crack fns at tip 1)}, \\ \texttt{crack\_bimat\_tip\_2} & \text{(Heaviside + bimat crack fns at tip 2)}, \end{cases}$$

where the last two definition are for the bimaterial crack problem. A sample input file used for the extended finite element analysis in Dynaflow™ is available from the web site: http://dilbert.engr.ucdavis.edu/~suku/xfem/dynaflow/input_dyna.dat.

3.2. Nodal degrees of freedom

In the finite element implementation for problems in 2-d linear elasticity, there are two unknowns at each node ($ndof = nsd = 2$). These correspond to the nodal displacements in each coordinate-direction. In the extended finite element, as is evident from Eq. (8), apart from the classical degrees of freedom, additional unknown enriched degrees of freedom are introduced via the displacement approximation. A Galerkin procedure is used to solve for both, the classical as well as enriched degrees of freedom. Since these enriched degrees of freedom are intrinsically based on the support properties of the shape functions associated with the original nodes in the mesh, it is natural to associate these unknown coefficients to the nodes themselves. In higher-order finite elements (bi-quadratic, bi-cubic, etc.), unknowns are tied to additional nodes that are introduced along the element edges.

Arrays are assumed to start with 1 unless otherwise indicated. In Dynaflow™, the nodal integer array `Id` is used to map a specific classical degree of freedom of a node to the global equation number. For the classical finite element method, the array is: $\mathtt{Id}(1 : ndof, 1 : nnode) = P$, where P is the global equation number. To accommodate the enriched degrees of freedom, a new integer array was defined for the enrichment: $\mathtt{IdX}(1 : ndof, 1 : ndofX, 1 : nnode) = P$, where the first slot is for the number of spatial degrees of freedom. In addition, $ndofX$ is the maximum number of enriched degrees of freedom in each coordinate direction, and $nnode$ is the number of nodes in the mesh. The array `Id` could have very easily been expanded to accommodate the enrichment; however, to reduce the likelihood of any conflict with existing applications, we chose to use a different array `IdX` for the enriched degrees of freedom. The value of $ndofX$ can be specified in the input data file within the DEFINE_PROBLEM block. If it is not specified in the data file, the value of $ndofX$ is inferred based on the `enrichment_type` indicated in the data file. For example, if `enrichment_type = Heaviside`, then $ndofX = 1$, but if `enrichment_type = crack`, then $ndofX = 4$ since a node cannot have both Heaviside and near-tip enrichment. In the event of multiple cracks, this variable should be appropriately set since it is possible that more than one crack may intersect the same element.

Now, the array `IdX` alone is not sufficient to fully quantify the enrichment for a crack. Since the appeal of the X-FEM is in the treatment of multiple cracks within the same framework, one must allow for the existence of multiple cracks within the same domain. Hence, by extension from the single crack case, when multiple cracks are present, separate nodal enrichment is required to ensure the presence of each crack in the domain. It follows that the enriched degrees of freedom at a node must be tied to a *crack id*, which would permit the computation of the appropriate enrichment function. This suggests the need to provide an additional data structure—a key which maps the degree of freedom information to a particular crack. This `character*20` array is dimensioned as: $\mathtt{Xdof\_key}(1 : ndof, 1 : ndofX, 1 : nnode)$. The *name* of the enrichment function is stored in the first to the eighteenth character (*name* is distinct for the two crack-tips), the nineteenth character is the enrichment function number ($\alpha = 1$–4 for the near-tip functions) and the twentieth character is the *crack id*. The `Xdof_key` array is filled-up when the enriched nodes are selected. A simple concatenation is done using the `char` function, for example 'Heaviside_crack_id'//char(ifunc)//char(crack_id)), and the extraction is done using the `ichar` function. Thus, for a direction $idof$ $(1 : ndof)$ with enrichment $idofX$ $(1 : ndofX)$ at node I, the corresponding equation number is obtained as $P = \mathtt{IdX}(idof, idofX, I)$, and the enrichment function number and crack number are $func\_id = \mathtt{ichar}(key(19 : 19))$ and $crack\_id = \mathtt{ichar}(key(20 : 20))$, respectively, where $key = \mathtt{Xdof\_key}(idof, idofX, I)$.

3.3. Mesh–geometry interaction

In 2-d, the finite element mesh consists of triangular and quadrilateral elements, and the crack is represented as a union of line segments with the crack-tip represented by a point. In the earlier 2-d (Daux et al., 2000) and 3-d (Sukumar et al., 2000) implementation of the X-FEM, the use of geometric predicates was

adopted. These also form an integral part in this work. In the following subsection, we discuss the concept of geometric predicates. In carrying out the enrichment, one of the first tasks is to determine the finite elements that intersect the crack. These finite elements are partitioned into triangles, which serves a dual purpose—first to compute the areas of the subtriangles above and below the crack (area-criterion in Section 2.1.2), and secondly so that the numerical integration of the bilinear form accounts for the discontinuities on either side of the crack.

3.3.1. Geometric predicates

Since data is stored and computations performed using finite-precision arithmetic, it is essential that the robustness of algorithms is maintained even for small perturbations in the data. Efforts have been made to develop robust geometric predicates (Shewchuk, 1997), which are especially important in the development of algorithms for the Delaunay tessellation and Voronoi diagram of a point set.

The *incircle* and *orientation* tests are widely used in computational geometry. The orientation test determines whether a point lies to the left of, to the right of, or on a line or plane defined by other points. The incircle test determines whether a point lies inside, outside, or on a circle defined by other points. Each of these tests is performed by evaluating the sign of a determinant. If the value of the determinant is close to zero, then computing the intersection of line segments is error-prone—on using single-precision or double-precision data, round-off errors could lead to an erroneous result or even failure in the intersection algorithm. Instead of explicitly computing intersections, geometric predicates provide an easier and robust means to evaluate queries.

In the X-FEM implementation, we adopt the orientation test to determine the nodal enrichment for a query point $\mathbf{x}$ and also use it in the algorithm for the partitioning of the finite elements into triangles. For a query point $\mathbf{x} \equiv (x, y)$, we consider the triangle with vertices $(\mathbf{x}_1, \mathbf{x}_2, \mathbf{x})$, where $\mathbf{x}_1 \equiv (x_1, y_1)$ and $\mathbf{x}_2 \equiv (x_2, y_2)$ are the coordinates that define a crack segment. Twice the signed area of the triangle (determinant Δ) is evaluated:

$$\Delta = (x_1 - x)(y_2 - y) - (x_2 - x)(y_1 - y). \tag{21}$$

To test the orientation of a point with respect to the crack, the ternary predicates `ABOVE` ($\Delta > \epsilon$) , `BELOW` ($\Delta < -\epsilon$), and `ON` ($-\epsilon \leqslant \Delta \leqslant \epsilon$) are used. A tolerance $\epsilon = 10^{-6}$ is used for a finite element mesh with element edge length of $\mathcal{O}(1)$.

3.3.2. Nodal enrichment and element partitioning

We first discuss the selection of the enriched nodes, then touch upon the computation of enrichment functions, and lastly discuss the partitioning of the finite elements that are intersected by the crack. To select the nodes for enrichment, a loop over the cracks and then over all the elements in the mesh suffices. A bounding-box algorithm that returns all the elements (set $\mathscr{E}$) in the vicinity of the crack proves to be computationally efficient. In Fig. 8, a flowchart illustrating the selection of enriched nodes for a single crack c is presented. The nodal enrichment information is stored in the `Xdof_key` array.

The computation of the enrichment functions is straight-forward. For a Gauss point $\mathbf{x}$ in an enriched element e, the binary predicates `ABOVE` ($H = 1$) and `BELOW` ($H = -1$) provide the value of H. The derivative of H is zero at a Gauss point. To compute the near-tip enrichment functions, the local crack-tip coordinate $(x_{\text{loc}}, y_{\text{loc}})$ of $\mathbf{x}$ is determined. Using these, the polar coordinates are: $r = \sqrt{x_{\text{loc}}^2 + y_{\text{loc}}^2}$ and $\theta = \tan^{-1}(y_{\text{loc}}/x_{\text{loc}})$. The derivatives of the near-tip enrichment functions are found in the local coordinate system and a vector transformation is used to obtain their derivatives with respect to the global (x, y) Cartesian coordinate system.

The element partitioning algorithm adopted in Daux et al. (2000) is described in Sukumar et al. (2000); the C++ code is also available in the public-domain (Sukumar, 2000). The C++ code was converted to

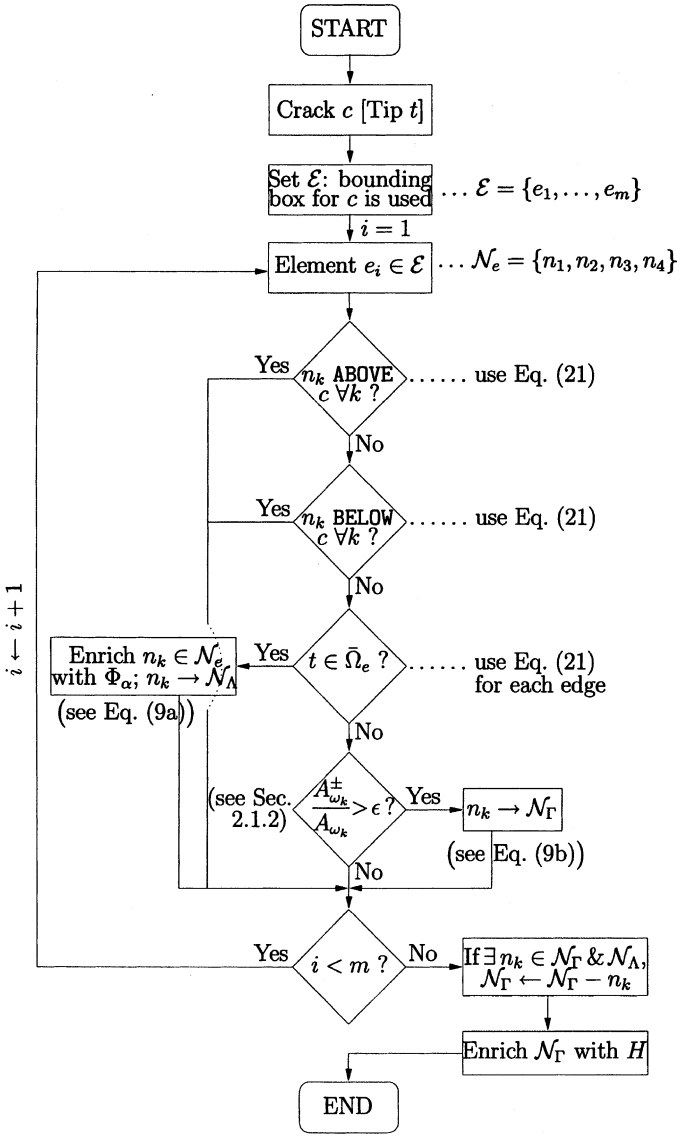

Fig. 8. Flowchart for selection of nodes for enrichment.

Fortran and implemented in Dynaflow™, with a few notable additions. We have implemented a tree data structure in conjunction with a linked list to permit the partition of a finite element that has a kink within it or one that is intersected by more than one crack. Geometric predicates and simple line–line intersection routines are used. An example illustrating the partitioning algorithm is shown in Fig. 9.

3.4. Assembly procedure

The stiffness matrix and force vector assembly are done on an element level, which is similar to classical finite element implementation. The distinction herein is that the dimensions of the element stiffness matrix

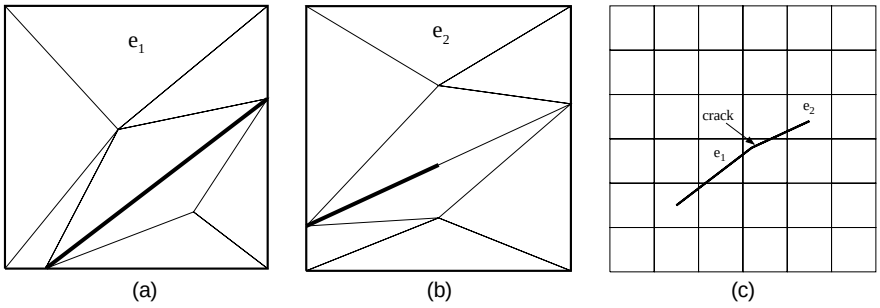

Fig. 9. Partitioning of finite elements in 2-d. (a) Finite element mesh and crack geometry; (b) Partitioning of element e_1 that is intersected by the crack (dark line); and (c) Partitioning of element e_2 that is intersected by the crack (dark line).

can differ from element (unenriched) to element (enriched). In our implementation, the element partitioning is done when required and the subtriangles are not stored; in Moës et al. (1999) and Daux et al. (2000), the partitioning was a pre-processing step and all the subtriangles were stored.

To assemble the stiffness matrix, we loop over all the elements, $e = 1 : \mathit{numel}$. If the IdX entry for a node is non-zero, then the node is enriched; if all the nodes in an element are not enriched, the element is a standard finite element and the element stiffness matrix for a 3-node triangular or 4-node quadrilateral element is computed. If the element e contains at least one enriched node, then the contribution in the stiffness matrix due to the classical degrees of freedom as well as the enriched degrees of freedom are evaluated—both contributions are stored in a single element stiffness matrix.

Elements that are partitioned require special treatment: as indicated before, partitioning is needed to ensure the equivalence between the strong form and the weak form and in addition it is also used to accurately integrate the bilinear form on either side of the crack discontinuity. Special (higher-order) quadrature rules are used on elements that are partitioned (Moës et al., 1999). On elements that are partitioned, a six-point integration rule is used in the subtriangles. In Fig. 9, a structured (rectangular) mesh containing an arbitrarily oriented crack is shown. The crack intersects some of the finite elements, and the subtriangles formed for elements e_1 and e_2 are illustrated in Fig. 9b and c. A finite element (*parent*) is denoted by e_q, whereas $e_q^\triangle$ is used for a subtriangle (*child*) that belongs to e_q. For an element e_q that has been partitioned, we loop over all its *children* (subtriangles). The isoparametric mapping for each Gauss point $\boldsymbol{\xi}_q^\triangle \in e_q^\triangle$ gives the global coordinate: $\mathbf{x} = \sum_{i=1}^{3} N_i^\triangle(\boldsymbol{\xi}_q^\triangle)\mathbf{x}_i^\triangle$. Now, since the degrees of freedom (classical as well as enriched) are defined on the *parent* (4-node) element, the local coordinate $\boldsymbol{\xi}_\square$ ($\square$ is the reference bi-unit square) is required to evaluate the derivatives of the finite element shape functions. To this end, an inverse map $\boldsymbol{\xi}_\square = \mathbf{x}^{-1}(\boldsymbol{\xi}_\square)$ from the global to the local coordinate-system is performed. The sequence of steps at a Gauss point in a subtriangle are: $\boldsymbol{\xi}_q^\triangle \to \mathbf{x} \to \boldsymbol{\xi}_\square$. Once $\boldsymbol{\xi}_\square$ is computed, Eqs. (19) and (20) are used to evaluate the contributions to the stiffness matrix. In Appendix A, we provide a listing of the subroutine used to compute $\boldsymbol{\xi}_\square$ in 2-d and 3-d.

A description of the update of the global stiffness matrix from the element stiffness matrix is outlined. The element connectivity array $\mathtt{IEN}(\mathit{nen}, e)$ contains the mapping from the local node number to the global node number, i.e., $I = \mathtt{Ien}(i, e)$, where I is the global node number, i is the local node number ($i = 1, \mathit{nen}$), and nen is the number of nodes in the connectivity of element e. Using $\mathtt{IEN}(\mathit{nen}, e)$, we localize the global equation numbers from the Id/IdX arrays into a local equation array $\mathtt{LM}(\mathit{ndof}, 0 : \mathit{ndofX}, \mathit{nen})$ as:

$$\mathtt{LM}(\mathit{idof}, 0, i) = \mathtt{Id}(\mathit{idof}, \mathtt{IEN}(i, e)), \tag{22a}$$

$$\mathtt{LM}(\mathit{idof}, \mathit{idofX}, i) = \mathtt{IdX}(\mathit{idof}, \mathit{idofX}, \mathtt{IEN}(i, e)). \tag{22b}$$

The element stiffness matrix and element force vector are assembled into local arrays `ke` and `fe` with dimensions `ke`(nee, nee) and `fe`(nee), respectively, where the dimension $nee = ndof\,(1 + ndofX)nen$. The assembly of the local stiffness matrix and the external force vector for element e proceeds in a straightforward and classical fashion in which `ke` and `fe` are passed to assembly routines where looping over the local equation numbers is carried out:

```
do p = 1, nee
   P = LM(p)
   if (P > 0) then
      do q = 1, nee
         Q = LM(q)
         if (Q > 0) then
            K(P,Q) = K(P,Q) + ke(p,q)
         endif
      enddo
      f(P) = f(P) + fe(p)
   endif
end
```

3.5. Post-processing

In the X-FEM, the degrees of freedom in unenriched elements are synonymous with nodal displacements. However, the classical degrees of freedom in an enriched element are in general no longer the nodal displacement—the nodal displacement is found by evaluating Eq. (8) at an enriched node. Since displacement plots are required to check the presence of the discontinuity and also to plot the deformed shape, it is desirable to expedite the evaluation of the displacement at the nodes. To this end, the values of the enrichment functions at the nodes are stored in an array. Since $H(\mathbf{x})$ is undefined at a node (say n_I) that lies on the crack, the enrichment function is multi-valued (+1 and −1). This also applies to the first near-tip function in Eq. (2), namely $\sqrt{r}\sin(\theta/2)$, which is discontinuous across the crack ($\theta = \pm\pi$). Since nodal output is element-based, in both cases, the appropriate sign is selected by knowing the element e under consideration ($n_I \in \mathcal{N}_e$). A simple check using the geometric predicates at $\mathbf{x}_c$ (center of element e) provides (`ABOVE` or `BELOW`) the sign to be used.

Fracture parameters such as the mode I and mode II stress intensity factors (SIFs) are determined using the domain form (Li et al., 1985; Moran and Shih, 1987) of the interaction integral (Yau et al., 1980). In the X-FEM, due to the enrichment with the near-tip fields, the SIFs can be expressed as a linear combination of the enriched coefficients. If the crack-tip Λ_c is inside an element e, then for a pure mode I problem in 2-d, the expression for K_I is:

$$K_I = \frac{E\sqrt{2\pi}}{4(1-\nu^2)} \sum_{i=1}^{nen} N_i(\mathbf{x}) b_{2i}^1, \quad \mathbf{x} \in \Lambda_c, \tag{23}$$

where N_i is the finite element shape function for node i, and b_{2i}^1 are enriched coefficients that are tied to the near-tip function Φ_1 and to the displacement approximation in x_2-direction. However, extraction of the SIFs directly from these coefficients is not sufficiently accurate. In general, the use of crack-tip flux integrals leads to better accuracy than even extrapolation (displacement or stress) techniques. In the domain integral form of the interaction integral, the numerical computations are carried out in elements (by appropriate choice of the weighting function) that are distant from the crack-tip; in these elements the field quantities are much more accurate than those in the vicinity of the crack-tip. For SIF computations, the domain form

of path-independent flux integrals is also used in commercial finite element codes (e.g., ABAQUS™); we adopt the same approach for the computation of stress intensity factors in this implementation. The J-integral is related to the mixed mode SIFs through the relation:

$$J = \frac{K_I^2}{E^*} + \frac{K_{II}^2}{E^*}, \quad E^* = \begin{cases} E & \text{(plane stress)}, \\ \dfrac{E}{1-\nu^2} & \text{(plane strain)}, \end{cases} \tag{24}$$

where E and ν are the Young's modulus and Poisson's ratio, respectively.

In the interaction integral method (Yau et al., 1980), the 2-d plane strain auxiliary fields are introduced and superposed on the actual fields that arise from the solution of the boundary-value problem. By judicious choice of the auxiliary fields, the interaction integral can be directly related to the mixed-mode stress intensity factors. The domain form of the interaction integral is computed on these elements (Yau et al., 1980). The domain form of the interaction integral is a well-established technique to determine mixed-mode SIFs in fracture computations with the finite element method. All the finite elements within a radius of $r_d = r_k h_e$ from the crack-tip are selected. Here, h_e is the crack-tip element size and r_k is a scalar multiple. All elements within a radius of r_d from the crack-tip are marked. Let us denote this element set by $\mathscr{N}_e^d$, with Ω_d^h defining the resulting discrete (union of elements) domain. The weighting function q that appears in the domain form of the interaction integral is then set: if a node n_i that is contained in the connectivity of element $e \in \mathscr{N}_e^d$ lies on the boundary $\partial\Omega_d^h$, then $q_i = 0$; if node n_i lies in Ω_d^h, then $q_i = 1$. Since the gradient of q appears in the domain integral expression, non-zero contribution to the integral in the numerical computations is obtained only for elements with an edge that lies on $\partial\Omega_d^h$. For additional details on the evaluation of the SIFs in the X-FEM, see Moës et al. (1999).

Some of the well-known crack growth criteria are: maximum hoop (circumferential) stress criterion (Erdogan and Sih, 1963); maximum energy release rate criterion (Nuismer, 1975); and the maximum strain energy density criterion (Sih, 1974). These criteria predict slightly different angles for the initial kink, but they all predict that once the kink is initiated, the crack trajectory is such that $K_{II} = 0$ (principle of local symmetry). The maximum hoop stress criterion (Erdogan and Sih, 1963) gives the crack growth direction:

$$\theta_c = 2\tan^{-1}\frac{1}{4}\left(\frac{K_I}{K_{II}} \pm \sqrt{\left(\frac{K_I}{K_{II}}\right)^2 + 8}\right), \tag{25}$$

where θ_c is the crack growth angle in the local crack-tip coordinate system. If $K_{II} = 0$ then $\theta_c = 0$ (pure mode I). By noting that if $K_{II} > 0$, the crack growth angle $\theta_c < 0$, and if $K_{II} < 0$, then $\theta_c > 0$, a computationally more amenable expression for θ_c is implemented (Suo, 2002):

$$\theta_c = 2\tan^{-1}\left[\frac{-2K_{II}/K_I}{1+\sqrt{1+8(K_{II}/K_I)^2}}\right], \tag{26}$$

where $\psi = \tan^{-1}(K_{II}/K_I)$, the mode angle, is a measure of the ratio of mode II to mode I. The application of the X-FEM to crack growth problems is presented in Part II (Huang et al., 2003b), which follows this publication.

4. Conclusions

In this paper (Part I of a two-part series), we have demonstrated a simple and robust means to implement the modeling of discontinuous fields within an existing finite element program. The methodology adopted for modeling crack discontinuities falls within the purview of the extended finite element method

(X-FEM) (Moës et al., 1999; Daux et al., 2000), which is a particular instance of the partition of unity method (Melenk and Babuška, 1996; Duarte and Oden, 1996). The finite element program Dynaflow™ (Prévost, 1983) was used in this study, and the implementation for crack modeling in isotropic and bi-material media was described. Issues pertaining to the selection of nodes for enrichment, computation of the enrichment functions, array-allocation for the enriched nodal degrees of freedom, mesh–geometry interactions, and assembly of the global stiffness matrix and external force vector were addressed. This study has provided the capability and revealed the relative ease by which discontinuous fields through the partition of unity framework can be incorporated within a standard finite element package.

Acknowledgements

The financial support to J.-H.P. from the National Science Foundation through contract NSF-9988788, Dr. Jorn Larsen-Basse Program Manager, is gratefully acknowledged. This work was accomplished in Spring 2001 when N.S. was visiting Princeton University; the hospitality extended to him by Professor David Srolovitz is appreciated. The comments and suggestions of the anonymous reviewers are also acknowledged.

Appendix A

Assume that a quadrilateral element which is cut by a crack is partitioned into triangular elements. The bilinear form (stiffness matrix) is computer over each subtriangle. On knowing the physical coordinates (x,y) of a point within a subtriangle, the local coordinates $(\xi,\eta)_{\square}$ ($\square$ is the bi-unit square that is mapped to the quadrilateral) are required to compute the finite element shape functions and their derivatives. The Fortran code to carry out the transformation follows; a Newton–Raphson iterative algorithm is used.

```
c*******************************************************************
      subroutine inversemap(xy,x,xe,nsd,nen,topo)
c  Purpose: Compute the inverse mapping from the physical space to
c  ===== the reference element for 2-d and 3-d finite elements
c
c  Input
c  ===
c  nodal coordinates : xy(nsd,nen)
c  coordinates : x(nsd) in physical space
c  topo : character array (topology of the element)
c  nsd = number of space dimensions, nen = number of nodes/element
c  Output
c  ===
c  local coordinates: xe(1) = xi, xe(2) = eta, xe(3) = zeta in the
c  reference bi-unit square/cube
c*******************************************************************
c
      implicit real*8 (a-h,o-z)
      parameter (Nsd_max=3, Nen_max=8)
c
      character*(*) topo
      dimension xy(nsd,*), x(*), xe(*)
```

```
      dimension xs(Nsd_max*Nsd_max), sh((Nsd_max+1)*Nen_max)
      dimension point(Nsd_max), xe_new(Nsd_max)
      parameter (iter_max=50, err_tol=1.d-8)
      nshp=nsd+1
c
c  initialize
      iter=0
      call dclear(xe,nsd) !clear the array
1     iter=iter+1
c
c  get shape functions at xe
      call shapl(xe,sh,nen,nshp,nsd,0,topo)
c
c  compute inverse of the jacobian map
      call xjacobian(xs,xy,nsd,sh,nshp,nen)
c
c  compute coordinates of point
      call dclear(point,nsd)
      do i=1,nsd
        do j=1,nen
          point(i)=point(i)+sh((nsd+1)+nshp*(j-1))*xy(i,j)
        enddo
      enddo
c
c  update xe
      do i=1,nsd
        xe_new(i)=xe(i)
        do j=1,nsd
          xe_new(i)=xe_new(i)+xs(i+nsd*(j-1))*(x(j)-point(j))
        enddo
      enddo
c
c  error
      do i=1,nsd
        xe(i)=xe_new(i)-xe(i)
      enddo
      err=sqrt(dotl(xe,xe,nsd)) !dotl (function for dot product)
      calldmove(xe,xe_new,nsd) !move xe_new to xe
      if (err.le.err_tol) then
        goto 99
      elseif (iter.lt.iter_max) then
        goto 1
      else
        call pend('inversemap: convergence failed') !error message
      endif
99    return
      end
c**********************************************************************
```

```
      subroutine xjacobian(xs,xl,nsd,sh,nshp,nen)
c     Purpose: Compute the inverse of the jacobian map
c     Output
c     ===
c     xs(nsd,nsd) : inverse of the jacobian map
c*********************************************************************
c
      implicit real*8 (a-h,o-z)
      dimension xs(nsd,*), xl(nsd,*), sh(Nshp,*)
      dimension cof(3,3), xinv(3,3)
      parameter (zero=0.d0, one=1.d0)
      call dclear(xs,nsd*nsd)
      do i=1,nsd
        do j=1,nsd
          do k=1,nen
            xs(i,j)=xs(i,j)+xl(i,k)*sh(j,k)
          enddo
        enddo
      enddo
      if (nsd.eq.2) then
        det=xs(1,1)*xs(2,2)-xs(1,2)*xs(2,1)
        if (det.le.zero) call pend('xjacobian: det.le.0')
        call dotacl(xs,one/det,nsd*nsd)
        tmp=xs(1,1)
        xs(1,1)=xs(2,2)
        xs(2,2)=tmp
        xs(1,2)=-xs(1,2)
        xs(2,1)=-xs(2,1)
      else
        COF(1,1)=XS(2,2)*XS(3,3)-XS(3,2)*XS(2,3)
        COF(1,2)=XS(2,3)*XS(3,1)-XS(2,1)*XS(3,3)
        COF(1,3)=XS(2,1)*XS(3,2)-XS(3,1)*XS(2,2)
        COF(2,1)=XS(3,2)*XS(1,3)-XS(1,2)*XS(3,3)
        COF(2,2)=XS(1,1)*XS(3,3)-XS(3,1)*XS(1,3)
        COF(2,3)=XS(3,1)*XS(1,2)-XS(1,1)*XS(3,2)
        COF(3,1)=XS(1,2)*XS(2,3)-XS(2,2)*XS(1,3)
        COF(3,2)=XS(2,1)*XS(1,3)-XS(1,1)*XS(2,3)
        COF(3,3)=XS(1,1)*XS(2,2)-XS(2,1)*XS(1,2)

        det=XS(1,1)*COF(1,1)+XS(1,2)*COF(1,2)+XS(1,3)*COF(1,3)
        if (det.le.zero) call pend('xjacobian: det.le.0')

        call dotacl(xs,one/det,nsd*nsd)
        XINV(1,1)= (XS(2,2)*XS(3,3)-XS(3,2)*XS(2,3))
        XINV(1,2)=-(XS(1,2)*XS(3,3)-XS(3,2)*XS(1,3))
        XINV(1,3)= (XS(1,2)*XS(2,3)-XS(2,2)*XS(1,3))
        XINV(2,1)=-(XS(2,1)*XS(3,3)-XS(3,1)*XS(2,3))
        XINV(2,2)= (XS(1,1)*XS(3,3)-XS(3,1)*XS(1,3))
```

```
      XINV(2,3) = -(XS(1,1)*XS(2,3) - XS(2,1)*XS(1,3))
      XINV(3,1) =  (XS(2,1)*XS(3,2) - XS(3,1)*XS(2,2))
      XINV(3,2) = -(XS(1,1)*XS(3,2) - XS(3,1)*XS(1,2))
      XINV(3,3) =  (XS(1,1)*XS(2,2) - XS(2,1)*XS(1,2))
      call dmove(xs,xinv,nsd*nsd)
    endif
c
    return
    end
```

References

Armero, F., Garikipati, K., 1996. An analysis of strong discontinuities in multiplicative finite strain plasticity and their relation with the numerical simulation of strain localization in solids. International Journal of Solids and Structures 33, 2863–2885.

Ayhan, A.O., Nied, H.F., 2002. Stress intensity factors for three-dimensional surface cracks using enriched finite elements. International Journal for Numerical Methods in Engineering 54 (6), 899–921.

Belytschko, T., Black, T., 1999. Elastic crack growth in finite elements with minimal remeshing. International Journal for Numerical Methods in Engineering 45 (5), 601–620.

Belytschko, T., Fish, J., Engelmann, B.E., 1988. A finite element with embedded localization zones. Computer Methods in Applied Mechanics and Engineering 70, 59–89.

Belytschko, T., Lu, Y.Y., Gu, L., 1994. Element-free Galerkin methods. International Journal for Numerical Methods in Engineering 37, 229–256.

Belytschko, T., Moës, N., Usui, S., Parimi, C., 2001. Arbitrary discontinuities in finite elements. International Journal for Numerical Methods in Engineering 50 (4), 993–1013.

Benzley, S.E., 1974. Representation of singularities with isoparametric finite elements. International Journal for Numerical Methods in Engineering 8, 537–545.

Beuth, J.L., 1992. Cracking of thin bonded films in residual tension. International Journal of Solids and Structures 29, 1657–1675.

Bogy, D.B., 1971. On the plane elastostatic problem of a loaded crack terminating at a material interface. Journal of Applied Mechanics 38, 911–918.

Bolzon, G., Corigliano, A., 2000. Finite elements with embedded displacement discontinuity: a generalized variable formulation. International Journal for Numerical Methods in Engineering 49 (10), 1227–1266.

Borja, R., 2000. A finite element model for strain localization analysis of strongly discontinuous fields based on standard Galerkin approximation. Computer Methods in Applied Mechanics and Engineering 190, 1529–1549.

Camacho, G.T., Ortiz, M., 1996. Computational modeling of impact damage in brittle materials. International Journal of Solids and Structures 33, 2899–2938.

Chen, D.H., 1994. A crack normal to and terminating at a bimaterial interface. Engineering Fracture Mechanics 49 (4), 517–532.

Chessa, J., Smolinski, P., Belytschko, T., 2002. The extended finite element method (XFEM) for solidification problems. International Journal for Numerical Methods in Engineering 53 (8), 1959–1977.

Chopp, D.L., Sukumar, N., 2003. Fatigue crack propagation of multiple coplanar cracks with the coupled extended finite element method/fast marching method. International Journal of Engineering Science 41 (8), 845–869.

Cook, T.S., Erdogan, F., 1972. Stresses in bonded materials with a crack perpendicular to the crack. International Journal of Engineering Science 10, 677–697.

Daux, C., Moës, N., Dolbow, J., Sukumar, N., Belytschko, T., 2000. Arbitrary cracks and holes with the extended finite element method. International Journal for Numerical Methods in Engineering 48 (12), 1741–1760.

Dolbow, J., 1999. An Extended Finite Element Method with Discontinuous Enrichment for Applied Mechanics. Ph.D. thesis, Theoretical and Applied Mechanics, Northwestern University, Evanston, IL, USA.

Dolbow, J., Nadeau, J., 2002. On the use of effective properties for the fracture analysis of microstructured materials. Engineering Fracture Mechanics 69 (14–16), 1607–1634.

Dolbow, J., Moës, N., Belytschko, T., 2000a. Discontinuous enrichment in finite elements with a partition of unity method. Finite Elements in Analysis and Design 36, 235–260.

Dolbow, J., Moës, N., Belytschko, T., 2000b. Modeling fracture in Mindlin–Reissner plates with the extended finite element method. International Journal of Solids and Structures 57 (48–50), 7161–7183.

Dolbow, J., Moës, N., Belytschko, T., 2001. An extended finite element method for modeling crack growth with frictional contact. Computer Methods in Applied Mechanics and Engineering 190 (51–52), 6825–6846.

Duarte, C.A., Oden, J.T., 1996. An *H-p* adaptive method using clouds. Computer Methods in Applied Mechanics and Engineering 139, 237–262.

Duarte, C.A., Babuška, I., Oden, J.T., 1998. October generalized finite element methods for three dimensional structural mechanics problems. In: Atluri, S.N., O'Donoghue, P.E. (Eds.), Modeling and Simulation Based Engineering: Proceedings of the International Conference on Computational Engineering Science, vol. I, Atlanta, GA. Tech. Science Press, pp. 53–58.

Duarte, C.A., Hamzeh, O.N., Liszka, T.J., Tworzydlo, W.W., 2001. The element partition method for the simulation of three-dimensional dynamic crack propagation. Computer Methods in Applied Mechanics and Engineering 119 (15–17), 2227–2262.

Dundurs, J., 1969. Edge-bonded dissimilar orthogonal elastic wedges. Journal of Applied Mechanics 36, 650–652.

Dvorkin, E.N., Cuitiño, A.M., Gioia, G., 1990. Finite elements with displacement interpolated embedded localization lines insensitive to mesh size and distortions. International Journal for Numerical Methods in Engineering 30, 541–564.

Erdogan, F., Sih, G.C., 1963. On the crack extension in plates under plane loading and transverse shear. Journal of Basic Engineering 85, 519–527.

Fleming, M., Chu, Y.A., Moran, B., Belytschko, T., 1997. Enriched element-free Galerkin methods for crack tip fields. International Journal for Numerical Methods in Engineering 40, 1483–1504.

Gifford Jr., L.N., Hilton, P.D., 1978. Stress intensity factors by enriched finite elements. Engineering Fracture Mechanics 10, 485–496.

Gravouil, A., Moës, N., Belytschko, T., 2002. Non-planar 3D crack growth by the extended finite element and the level sets—Part II: level set update. International Journal for Numerical Methods in Engineering 53 (11), 2569–2586.

Huang, R., Prévost, J.H., Huang, Z.Y., Suo, Z., 2003a. Channel-cracking of thin films with the extended finite element method. Engineering Fracture Mechanics 70 (18), 2513–2526.

Huang, R., Sukumar, N., Prévost, J.-H., 2003b. Modeling quasi-static crack growth with the extended finite element method. Part II: numerical applications. International Journal of Solids and Structures, in this issue.

Hughes, T.J.R., 1987. The Finite Element Method. Prentice-Hall, Englewood Cliffs, NJ.

Ji, H., Chopp, D., Dolbow, J.E., 2002. A hybrid extended finite element/level set method for modeling phase transformations. International Journal for Numerical Methods in Engineering 54 (8), 1209–1233.

Jirásek, M., 2000. Comparative study on finite elements with embedded discontinuities. Computer Methods in Applied Mechanics and Engineering 188, 307–330.

Larsson, R., Runesson, K., 1996. Element-embedded localization band based on regularized displacement discontinuity. ASCE Journal of Engineering Mechanics 12, 402–411.

Larsson, R., Steinmann, P., Runesson, K., 1999. Finite element embedded localization band for finite strain plasticity based on a regularized strong discontinuity. Mechanics of Cohesive-Frictional Materials 4 (2), 171–194.

Li, F.Z., Shih, C.F., Needleman, A., 1985. A comparison of methods for calculating energy release rates. Engineering Fracture Mechanics 21 (2), 405–421.

Lotfi, H.R., Sheng, P.B., 1995. Embedded representations of fracture in concrete with mixed finite elements. International Journal for Numerical Methods in Engineering 38, 1307–1325.

Melenk, J.M., Babuška, I., 1996. The partition of unity finite element method: basic theory and applications. Computer Methods in Applied Mechanics and Engineering 139, 289–314.

Merle, R., Dolbow, J., 2002. Solving thermal and phase change problems with the extended finite element method. Computational Mechanics 28 (5), 339–350.

Moës, N., Belytschko, T., 2002. Extended finite element method for cohesive crack growth. Engineering Fracture Mechanics 69 (7), 813–833.

Moës, N., Dolbow, J., Belytschko, T., 1999. A finite element method for crack growth without remeshing. International Journal for Numerical Methods in Engineering 46 (1), 131–150.

Moës, N., Gravouil, A., Belytschko, T., 2002. Non-planar 3D crack growth by the extended finite element and level sets. Part I: mechanical model. International Journal for Numerical Methods in Engineering 53 (11), 2549–2568.

Moran, B., Shih, C.F., 1987. Crack tip and associated domain integrals from momentum and energy balance. Engineering Fracture Mechanics 27 (6), 615–641.

Nuismer, R., 1975. An energy release rate criterion for mixed mode fracture. International Journal of Fracture 11, 245–250.

Oden, J.T., Duarte, C.A., Zienkiewicz, O.C., 1998. A new cloud-based hp finite element method. Computer Methods in Applied Mechanics and Engineering 153 (1–2), 117–126.

Ortiz, M., Leroy, Y., Needleman, A., 1987. A finite element method for localized failure analysis. Computer Methods in Applied Mechanics and Engineering 61, 189–214.

Prévost, J.-H., 1983. Dynaflow. Princeton University, Princeton, NJ 08544 (updated version: 2002).

Rashid, M.M., Gullett, P.M., 2000. On a finite element method with variable element topology. Computer Methods in Applied Mechanics and Engineering 190 (11–12), 1509–1527.

Regueiro, R.A., Borja, R.I., 2001. Plane strain finite element analysis of pressure sensitive plasticity with strong discontinuity. International Journal of Solids and Structures 38 (21), 3647–3672.

Shewchuk, J.R., 1997. Adaptive precision floating-point arithmetic and fast robust geometric predicates. Discrete and Computational Geometry 18, 305–363.

Sih, G.C., 1974. Strain energy density factor applied to mixed mode crack problems. International Journal of Fracture 10, 305–321.

Simo, J.C., Oliver, J., 1994. Modelling strong discontinuities in solid mechanics by means of strain softening constitutive equations. In: Mang, H., Bićanić, N., de Borst, R. (Eds.), Computational Modelling of Concrete Structures. Pineridge, Swansea, pp. 363–372.

Simo, J.C., Oliver, J., Armero, F., 1993. An analysis of strong discontinuities induced by strain softening in rate-independent inelastis solids. Computational Mechanics 12, 277–296.

Sluys, L.J., Berends, A.H., 1998. Discontinuous failure analysis for mode-I and mode-II localization problems. International Journal of Solids and Structures 35, 4257–4274.

Stolarska, M., Chopp, D.L., Moës, N., Belytschko, T., 2001. Modeling crack growth by level sets and the extended finite element method. International Journal for Numerical Methods in Engineering 51 (8), 943–960.

Strouboulis, T., Babuška, I., Copps, K., 2000. The design and analysis of the generalized finite element method. Computer Methods in Applied Mechanics and Engineering 181 (1–3), 43–69.

Strouboulis, T., Copps, K., Babuška, I., 2001. The generalized finite element method. Computer Methods in Applied Mechanics and Engineering 190 (32–33), 4081–4193.

Sukumar, N., 2000. Element partitioning code in 2-d and 3-d for the extended finite element method. Available from <http://dilbert.engr.ucdavis.edu/~suku/xfem.

Sukumar, N., Moës, N., Moran, B., Belytschko, T., 2000. Extended finite element method for three-dimensional crack modeling. International Journal for Numerical Methods in Engineering 48 (11), 1549–1570.

Sukumar, N., Chopp, D.L., Moës, N., Belytschko, T., 2001. Modeling holes and inclusions by level sets in the extended finite-element method. Computer Methods in Applied Mechanics and Engineering 190 (46–47), 6183–6200.

Sukumar, N., Chopp, D.L., Moran, B., 2003a. Extended finite element method and fast marching method for three dimensional fatigue crack propagation. Engineering Fracture Mechanics 70 (1), 29–48.

Sukumar, N., Srolovitz, D.J., Baker, T.J., Prévost, J.-H., 2003b. Brittle fracture in polycrystalline microstructures with the extended finite element method. International Journal for Numerical Methods in Engineering 56 (14), 2015–2037.

Sukumar, N., Huang, Z.Y., Prévost, J.-H., Suo, Z., in press. Partition of unity enrichment for bimaterial interface cracks. International Journal for Numerical Methods in Engineering.

Suo, Z., 2002. Private communication.

Wagner, G., Moës, N., Liu, W.K., Belytschko, T., 2001. The extended finite element method for rigid particles in Stokes flow. International Journal for Numerical Methods in Engineering 51 (3), 293–313.

Wells, G.N., Sluys, L.J., 2001. A new method for modelling cohesive cracks using finite elements. International Journal for Numerical Methods in Engineering 50 (12), 2667–2682.

Wells, G.N., Sluys, L.J., deBorst, R., 2002. A p-adaptive scheme for overcoming volumetric locking during plastic flow. Computer Methods in Applied Mechanics and Engineering 191 (29–30), 3153–3164.

Xu, X.-P., Needleman, A., 1994. Numerical simulations of fast crack growth in brittle solids. Journal of the Mechanics and Physics of Solids 42, 1397–1434.

Yau, J.F., Wang, S.S., Corten, H.T., 1980. A mixed-mode crack analysis of isotropic solids using conservation laws of elasticity. Journal of Applied Mechanics 47, 335–341.

Zak, A.R., Williams, M.L., 1963. Crack point singularities at a bimaterial interface. Journal of Applied Mechanics 30, 142–143.